Dynamic and Thermodynamic Processes Related to Sea-Ice Surface Melt Advance in the Laptev Sea and East Siberian Sea

Hongjie LIANG, [1] Wen ZHOU [1,2]

[1] *Department of Atmospheric and Oceanic Sciences & Institute of Atmospheric Sciences, Fudan University, Shanghai, China*

[2] *Center for Polar Ice & Snow and Climate Change Research, Polar Research Institute of China, Shanghai, China*

Correspondence to: Wen Zhou (wen_zhou@fudan.edu.cn)

Aug, 2023

ABSTRACT

Arctic summer sea ice has shrunk considerably in recent decades. This study investigates springtime sea-ice surface melt onset in the Laptev Sea and East Siberian Sea, which are key seas along the Northeast Passage. Instead of region-mean melt onset, we define an index of Melt Advance, which is the areal percentage of a sea that has experienced sea-ice surface melting before the end of May. Four representative scenarios of Melt Advance in the region are identified. Each scenario is accompanied by a combination of distinct patterns between atmospheric circulation, atmospheric thermodynamic state, sea ice cover (polynya activity), and surface energy balance in May. In general, concurrent with faster Melt Advance are warmer and wetter atmosphere, less sea ice cover, and surface energy gains in spring. Melt Advance, like sea ice cover in May, is significantly correlated with summer sea ice cover. This study implicates the interannual and interdecadal flexibility of spring circulation in the lower troposphere and the significance of seasonal evolution in the Arctic.

1. Introduction

Since the 1970s, satellites have enabled global detection of the Earth. Arctic summer sea ice extent is found to have decreased dramatically in the past four decades (Petty et al., 2020; Stroeve and Notz, 2018), which is a prominent indicator of global warming. In fact, the Arctic has a faster warming trend than elsewhere on the planet, especially in the lower troposphere during the cold season(Cohen et al., 2014; Serreze et al., 2009; Screen and Simmonds, 2010). This phenomenon, called Arctic Amplification, presumably results from reduced sea ice cover and enhanced oceanic energy release toward the atmosphere, atmospheric and oceanic heat transport from lower latitudes, and local positive feedbacks (Serreze et al., 2009; Cohen et al., 2014; Taylor et al., 2022). Some research has indicated that the mid-latitudes may frequently experience severe winters due to the Arctic Amplification which reduces the meridional temperature gradient and in turn amplifies the planetary Rossby wave and makes it more stationary (Francis and Vavrus, 2015). In the Arctic, positive ice-albedo feedback is active in the melt season (Budyko, 1969; Kashiwase et al., 2017; Sellers, 1969): after sea ice begins to melt in spring, surface albedo decreases substantially, which favors more solar radiation absorption and promotes further sea ice melting. Based on this notion, some studies have tried to predict Arctic summer sea ice cover by sea-ice surface Melt Onset (MO) in spring, i.e., the date when the sea ice surface begins to form liquid water (Petty et al., 2017; Wang et al., 2011). Currently, satellite remote sensing helps us construct the pan-Arctic sea ice MO, which is not possible with only in-situ field observations. However, for sea ice lateral and bottom melting, satellites are less useful and buoys are widely employed (Lei et al., 2022).

Many studies have touched on sea ice MO in springtime (Drobot and Anderson, 2001; Bliss and Anderson, 2014; Horvath et al., 2021; Crawford et al., 2018; Markus et al., 2009; Stroeve et al., 2014). Generally, sea ice MO is becoming earlier in most parts of the Arctic, which is consistent with the Arctic warming. Another notable feature of MO is its regionality. For example, the Barents Sea, Kara Sea, Laptev Sea, and East Siberian Sea are around the same latitudes along the Siberian coast, but the MO trends were -7.1, -5.2, -2.8, and -1.8 days per decade from 1979 to 2013, respectively (Stroeve et al., 2014). Liang and Su (2021) investigated the interannual early/late relationship of MO between the Laptev Sea and East Siberian Sea, which is related to the large-scale atmospheric pattern of the Barents Oscillation (Skeie, 2000). Locally, synoptic processes are regarded as responsible for interannual variability. Mortin et al. (2016) argued that sea ice MO is generally associated with higher surface air temperature (SAT), total-column water vapor (TWV), and cloud cover, which promotes downward longwave radiation.

The Laptev Sea (LS) and East Siberian Sea (ESS) are marginal seas of the Arctic Ocean, north of Siberia along the Northeast Passage (Fig. S1). The longitude-latitude ranges are around 70°N-80°N and 100°E-180°, covering 0.66 and 1.14 million km^2 for the LS and ESS, respectively. These two seas are among the regions where sea ice decline in September during the past four decades has been the most prominent, and they are key regions for safe transportation across the Northeast Passage. In spring, sea ice almost completely covers the seas, while in summer, sea ice substantially retreats off the coast.

Focusing on the LS and ESS, which usually have the most persistent sea ice coverage in the Northeast Passage, this study aims to demonstrate the springtime processes related to different Melt Advance scenarios and explore the linkage between springtime Melt Advance and summertime sea ice coverage.

2. Data and Methods

Sea ice Melt Onset (MO) is the date when the sea ice surface begins to melt in spring, which is retrieved from satellite passive microwave signals (Markus et al., 2009). Liquid water has greater emissivity than ice/snow, so surface melting invokes changes in passive microwave signals. The dataset is distributed by the National Aeronautics and Space Administration (NASA) Cryospheric Sciences Research Portal. We use the yearly MO from 1979 to 2018, with a spatial resolution of ~25 km. Following the method in Liang and Su (2021), we fill in the missing MO values based on surface air temperature (SAT) datasets from the International Arctic Buoy Programme/Polar Exchange at the Sea Surface (IABP/POLES) for 1979-2004 and the Atmospheric InfraRed Sounder (AIRS) for 2005-2018. Although the missing values are not quite a lot, the analysis here is more convenient if the whole research area in the LS and ESS is covered.

The sea ice concentration (SIC) dataset, called Ocean and Sea Ice Satellite Application Facility (OSI SAF), is from the European Organization for the Exploitation of Meteorological Satellites (EUMETSAT) (Lavergne et al., 2019). We use the monthly SIC in May from 1979 to 2018, with a resolution of 25 km. We also examine SIC dataset by the NASA Team algorithm(Cavalieri et al., 1996), which shows basically the same patterns in May as OSI SAF.

The atmospheric variables and surface energy fluxes are from the ERA5 reanalysis by the European Centre for Medium-Range Weather Forecasts (ECMWF) (Hersbach et al., 2020), which replaces the ERA-Interim reanalysis that ceased production in 2019. The variables used in this study are monthly downward longwave radiation (DLR), net longwave radiation (NLR), downward shortwave radiation (DSR), net shortwave radiation (NSR), surface latent heat flux (SLHF), surface sensible heat flux (SSHF), total-column water vapor (TWV), and SAT and wind fields at the 850-hPa level, for the month of May from 1979 to 2018. The spatial resolution of ERA5 used in this study is 0.25°×0.25°, less than 30 km in the region of the Laptev Sea and East Siberian Sea. Note that the four components of the surface energy balance (SEB) include NLR, NSR, SLHF, and SSHF.

3. Results

3.1 Distinct Melt Advance Scenarios in the Laptev Sea and East Siberian Sea

Sea ice begins to melt at the surface in spring when solar radiation increases and the atmosphere warms. On average, the sea ice surface in the Laptev Sea (LS) and East Siberian Sea (ESS) begins to melt during May and June (Fig. 1a). Naturally, sea ice melting advances northward in a given year. The range for the interannual change of MO in a given place is expected to be around one month (Fig. 1b). In order to demonstrate the progress of MO in different years, melt advance (MA) is defined by calculating the areal percentage of an individual sea that has experienced MO at the end of May (see magenta contour line in Fig. 1a). In this way, we can detect whether sea-ice surface melting advances slowly or quickly in a specific year, as well as the spatial patterns of the melt advance. For the seasonal prediction of summer sea ice, this metric of Melt Advance is in essence similar to the average MO date, but may have advantages if we can get real-time satellite MO for the region. Then, at the end of May or other specific date, we can get the MA pattern which supports timely seasonal prediction.

Figure 1c shows the time series of MA for the LS and ESS during 1979-2018. The variability is large, ranging from near zero to 100%. This implies changeable spring conditions on the interannual scale. On average, MA is around 40% for each sea, meaning that ~40% of the sea area has experienced sea-ice surface melting at the end of May. In the context of global warming, MA has an increasing tendency in both seas although this tendency is not quite significant (less than 6% per decade). This indicates that we sometimes need to pay more attention to the interannual variability than to the long-term linear tendency. We can also notice that relatively slow MA in the 1980s contributes considerably to the overall positive tendency.

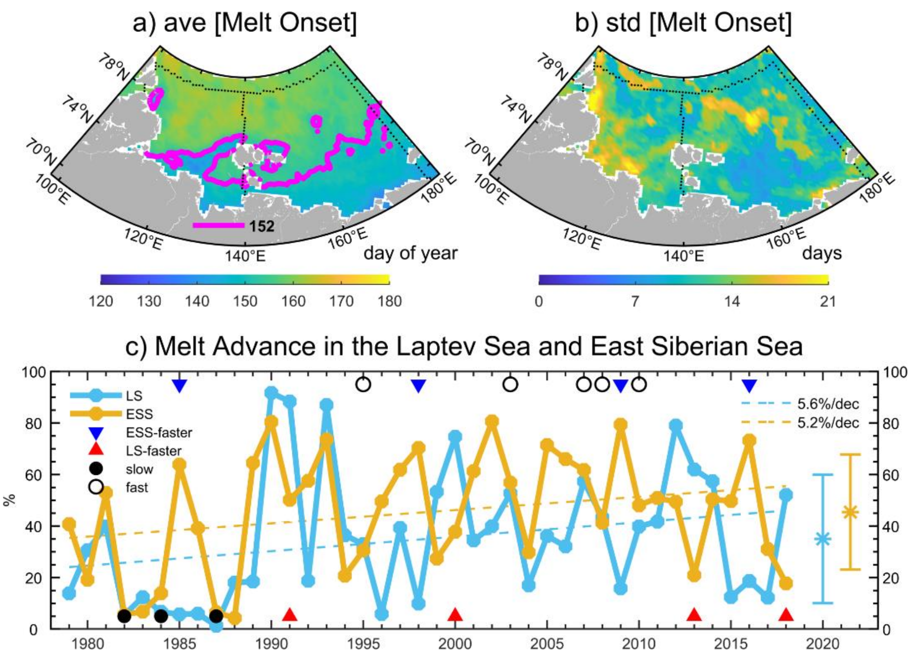

Fig. 1. (a, b) Climatology and standard deviation of sea ice Melt Onset, and (c) Melt Advance time series in the Laptev Sea and East Siberian Sea, 1979-2018. The magenta lines in panel (a) are contours of 152 (day of year), representing the end of May. The areal percentage of sea ice Melt Onset earlier than 152 (day of year) is defined as Melt Advance. In panel (c), only the trend of Melt Advance in the ESS is statistically significant at the 90% confidence level. The average and standard deviation of the Melt Advance in the LS and ESS are 35%±25% and 45%±22%, respectively. Sample years (16 out of the long time-series) that fall into one of four categories are marked (see also Table 1).

Another feature is related to the relationship of MA between the LS and ESS. In some years, MA in both the LS and ESS is slow, as in the 1980s; in other years, MA in both seas may be fast; and in other years, MA can be substantially different in the two seas. Thus, four categories of sample years are selected for further composite analysis (Table 1 and markers in Fig. 1c; MA difference between the LS and ESS is shown in Fig. S2), which represent four basic scenarios of MA in this region. Specifically, years with significantly faster MA in the ESS than in the LS (δ>48%) are grouped as the ESS-faster-scenario, while years with significantly faster MA in the LS than in the ESS (δ>33%) are classified as the LS-faster-scenario. The slow-scenario includes years when MA in both seas is slow (below 20%), while the fast-scenario consists of years when MA in both seas is relatively fast (between 30% and 60% at the same time). So, two pairs of contrasting categories are formed (ESS-faster-scenario vs. LS-faster-scenario, slow-scenario vs. fast-scenario). Note that to some extent the latter two scenarios represent the contrast between the 1980s and subsequent decades. Such categorization also reflects the large variability of MA in spring from the interannual perspective.

Category	Years	Description
ESS-faster-scenario	1985, 1998, 2009, 2016	significantly faster Melt Advance (δ>48%) in the ESS than in the LS
LS-faster-scenario	1991, 2000, 2013, 2018	significantly faster Melt Advance (δ>33%) in the LS than in the ESS
slow-scenario	1982, 1984, 1987	similar but slow Melt Advance (δ<8%, but below 20%)
fast-scenario	1995, 2003, 2007, 2008, 2010	similar but fast Melt Advance (δ<9%, but between 30% and 60%)

Table 1 List of years under different scenarios of Melt Advance.
Note: Practically, the ESS-faster-scenario and LS-faster-scenario are selected based on one standard deviation of the difference in Melt Advance between the Laptev Sea and East Siberian Sea. The slow-scenario and fast-scenario include years when Melt Advance in the two seas is quite close. All years listed here are marked in Fig. 1c.

Composite results show that the ESS-faster-scenario has substantially earlier MO, i.e., faster MA in the ESS than in the LS, while the LS-faster-scenario has a somewhat opposite signal (indicated by the magenta line in Fig. 2). For the slow-scenario, little area in either sea has experienced MO until the end of May, indicating slow MA; for the fast-scenario, nearly half of both seas has begun to experience sea-ice surface melting, indicating fast MA at almost the same pace. From the surface energy balance (SEB) in May, we find consistent patterns. With the zero lines of SEB as a reference, the ESS-faster-scenario has relatively more positive SEB in the ESS than in the LS, while the opposite is true for the LS-faster-scenario. For the slow-scenario, SEB is negative over most of the two seas, while for the fast-scenario, SEB is positive in both seas. This fits well with common sense. Although MA-related albedo changes may amplify the SEB signals in a two-way interaction, it is fair to say that SEB in May drives different patterns of MA (see individual years in Fig. S3).

In the next section, we investigate systematic processes under different MA scenarios that involve the atmosphere, sea ice, and surface energy fluxes.

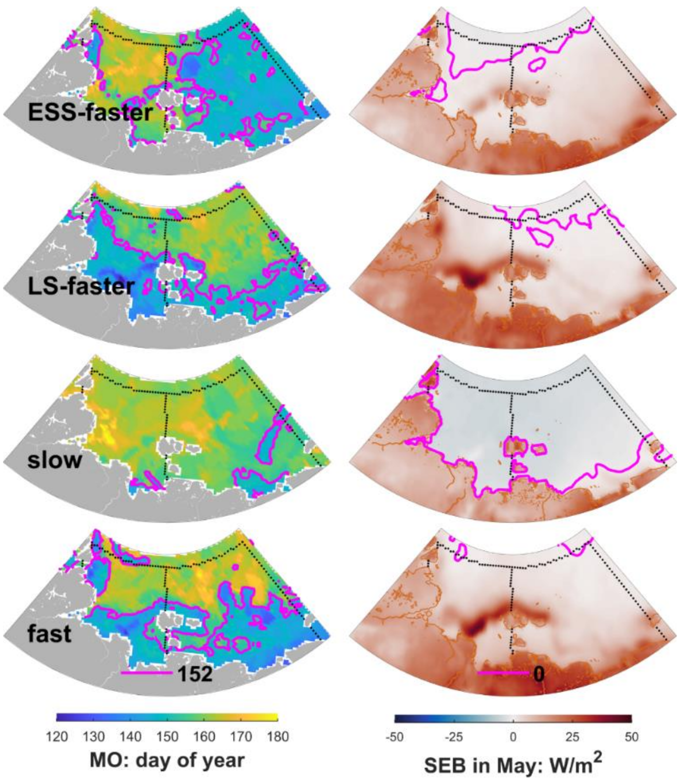

Fig. 2. Composites of MO and surface energy balance (SEB) in May for the four

scenarios. The left column shows the MO patterns marked by magenta contour lines with the value of 152 (day of year) which represents the end of May. The right column is the SEB in May, with magenta contour lines of zero. Black dots denote the boundaries of the LS and ESS.

3.2 Dynamic and Thermodynamic Processes under Different Melt Advance Scenarios

Climatologically, SEB is basically positive (~5 W/m^2) across the two seas in May (see first row in Fig. S4). Among the components, it is positive net shortwave radiation (NSR) that compensates for losses from net longwave radiation (NLR), SLHF, and SSHF. This implies that on average the atmosphere receives energy from the surface through the latter three components in May. SAT is around -6°C, while sea ice almost fully covers the ocean (~90%) (see first row in Fig. 3). In the lower troposphere (850 hPa), southeasterlies blow across the region, which to some extent explains the existence of polynyas in the middle LS, i.e., regions where sea ice concentration is below 75%. Note that Fig. 3 shows only selected vital variables; other relevant factors can be found in Fig. S4-S7.

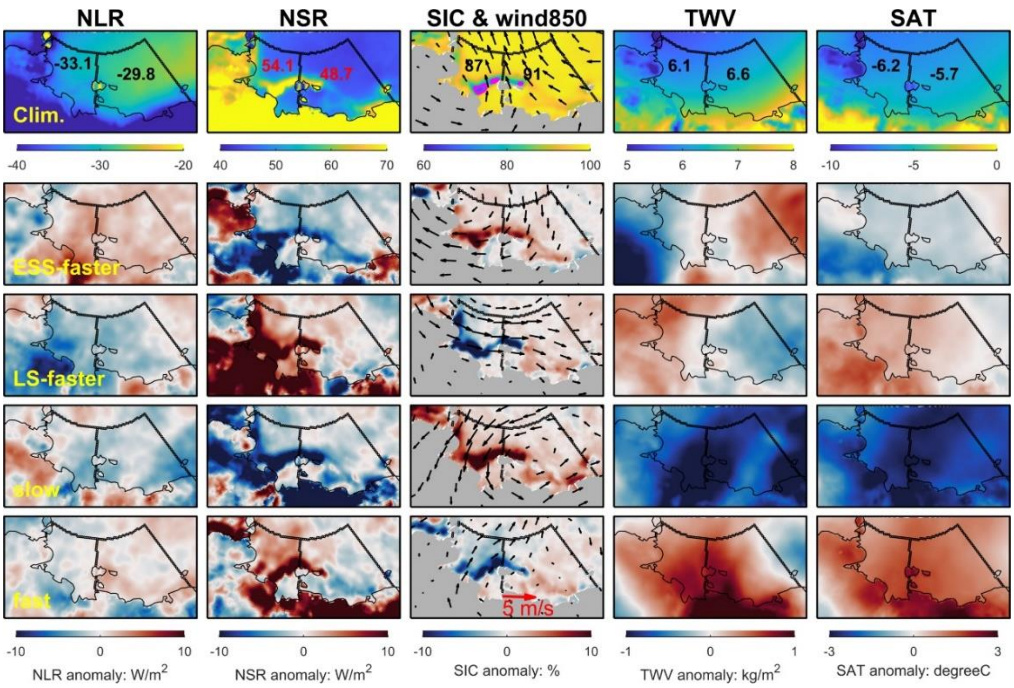

Fig. 3. Climatology (first row) and composite anomalies for the four scenarios (lower four rows) of relevant atmospheric and sea ice variables in May: NLR, NSR, SIC, winds at 850 hPa, TWV, and SAT. Numbers within the LS and ESS are the region-mean values,

respectively. Note that magenta lines in the climatological SIC fields denote contours of 75% SIC values, which suggest the location of polynyas.

In the ESS-faster-scenario (see second row in Fig. 3 and blue bars in Fig. 4), prevailing northeasterlies in the lower troposphere tend to increase SIC and reduce polynya area, especially for the LS, which increases surface albedo and decreases solar radiation absorption. The northeasterlies seem to also bring slightly cool air masses to the region, and slightly moist air masses to the ESS. Given that sea ice cover is more packed, longwave radiation loss from the surface to the atmosphere is reduced, which to some extent compensates for the reduced solar radiation absorption. Due to the greater negative anomaly of solar radiation absorption in the LS, the net surface energy balance is a loss in the LS, but a gain in the ESS (Fig. S4 and S6). In addition, sea-ice surface melting is usually preconditioned by increased water vapor in the atmosphere (Mortin et al., 2016). So, faster Melt Advance in the ESS is expected as TWV is increased in the ESS.

For the LS-faster-scenario (see third row in Fig. 3 and red bars in Fig. 4), wind fields at 850-hPa show unified westerlies over the LS and northwesterlies over the ESS, which to some extent account for the reduced sea ice cover in the LS and the slightly packed sea ice in the ESS. Such circulation has offshore wind component in the LS and drive sea ice out of the LS, which probably leads to more polynya opening and reduced SIC (Krumpen et al., 2011). So, we see a substantial increase in solar radiation absorption (beyond one standard deviation) in the LS. While longwave radiation loss is somehow enhanced, the net surface energy balance is still a gain for the LS and a loss for the ESS. The westerlies may also bring warm and wet air masses from the North Atlantic and contribute to positive anomalies of TWV and SAT in the LS, which promotes faster MA. We may expect that reduced sea ice cover in the LS enables more moisture to be released from the exposed ocean. However, latent heat loss as well as sensible heat loss toward atmosphere in the LS weakens (Fig. S4 and S6), which suggests that warmer and moister atmosphere is mainly a result of air mass transport and in turn reduces turbulent heat loss from the surface.

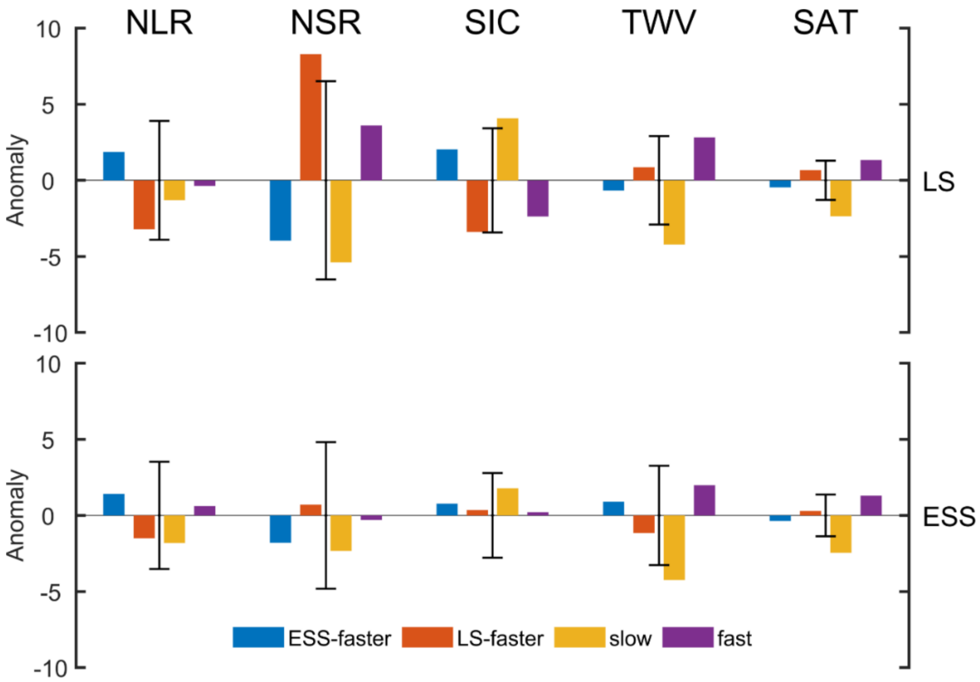

Fig. 4. Region-mean composite anomalies in the LS and ESS for the four scenarios shown in Fig. 3. The error bars denote the corresponding standard deviation for 1979-2018. The variables of NLR, NSR, SIC, TWV, and SAT have units of W/m^2, W/m^2, %, kg/m^2, and K, respectively. Here, SIC is represented by the areal percentage of sea ice cover relative to the whole sea. To facilitate viewing, TWV is scaled by a factor of 5.

For the slow-scenario (see fourth row in Fig. 3, and orange bars in Fig. 4), a cyclonic anomaly in the lower troposphere, which is centered on the ESS, pushes sea ice against the southern coast in the LS. More sea ice cover in both seas decreases solar radiation absorption. Meanwhile, this region is under the influence of cold and dry air masses (beyond one standard deviation), which induce a large loss of longwave radiation and SSHF from the surface. As a whole, we see unified surface energy deficits in the LS and ESS (beyond one standard deviation). Note that all the three sample years are from the 1980s. So, the larger sea ice cover and cooler atmosphere mainly reflect the Arctic state in the 1980s, which is a decadal phenomenon rather than interannual characteristics. We also examine the monthly snowfall under the four scenarios (Fig. S5). For this region, snowfall dominates the total precipitation in May. Especially for the slow melt advance scenario, snowfall is abnormally high, which will also result in high surface albedo.

For the fast-scenario, with sample years after the 1980s (see last row in Fig. 3, and purple bars in Fig. 4), southerlies in the lower troposphere blow mainly across the LS, which drive sea ice off the coast, open the polynya and in turn increase shortwave radiation absorption. At the same time, the southerlies bring warm and wet air masses to this region, which substantially reduce the SSHF loss from the surface. As a result, we see a positive net surface energy balance in this region and relatively fast MA.

The composite analysis above indicates that circulation in the lower troposphere in spring in this region can be quite changeable (see individual years in Fig. S8), which can have two effects: one is related to sea ice dynamics; the other involves moisture and air mass advection. The former produces strong regulation of NSR due to albedo changes, while the latter has everything to do with the atmospheric state, which favors sea-ice surface melting when the atmosphere is warm and wet.

Figure 5 further shows the statistical correlation related to MA, covering years from 1979 to 2018. In general, we see that faster MA is accompanied by warm and wet atmosphere. The related atmospheric circulation in the lower troposphere may also drive reduced SIC and subsequent increased solar radiation absorption. In addition, Mortin et al. (2016) argued that on a synoptic scale, increased water vapor in the atmosphere favors stronger DLR, which promotes sea-ice surface melting. Such conclusion makes sense when we focus on sea ice and atmosphere above. While we examine from the perspective of the whole region, including effects of the open ocean, results here suggest that on the subseasonal scale net longwave radiation has little connection with MA (see first column in Fig. 5). To some extent, the weak correlation even shows that on the monthly scale, longwave radiation loss tends to be more when SEB is more and MA is faster, which suggests some negative feedback probably related to the open ocean.

While NSR is strong, downward shortwave radiation tends to be less (see Fig. S9), which is expected from more moisture in the atmosphere. However, cloud analysis based on ERA5 reanalysis doesn't suggest significant effects of clouds. Total cloud cover in this region generally is larger than 90% in May and interannual anomaly is relatively small (less than 5%, see Fig. S5). This indicates that from the perspective of anomaly, water vapor rather than cloud cover has considerable radiation effects in the springtime. Given the large uncertainty of clouds in current datasets, this remains an open question.

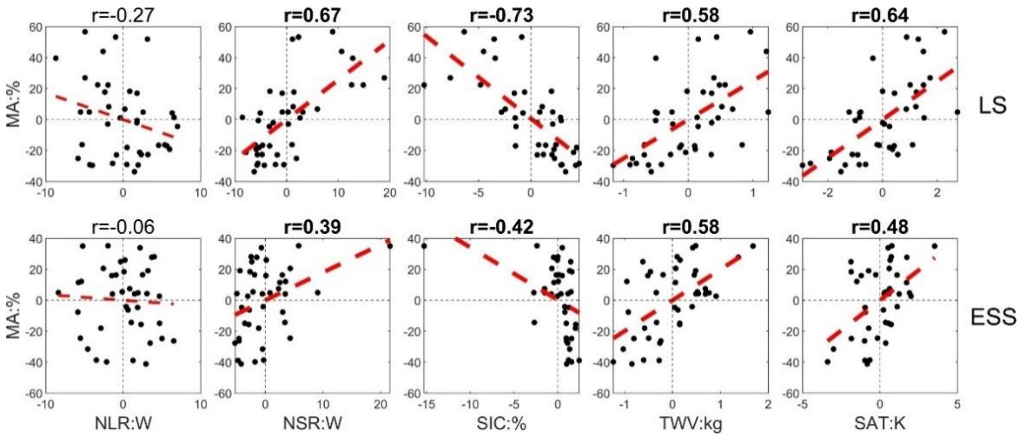

Fig. 5. Scatter plots for 1979-2018 between the MA anomaly and region-mean anomalies of factors shown in Figs. 3 and 4. Thick dashed red lines denote linear fits above the 95% confidence level. Bold titles represent correlation above the 95% confidence level.

To what extent do different sea-ice surface melting scenarios in spring have implications for sea ice cover in summer? Could we gain seasonal prediction skill based on detection of sea-ice surface melting in spring? A simple way to address this is to put aside the processes linking spring and summer and directly investigate the statistical relationship between sea-ice surface melting scenarios in spring and sea ice states in summer. Figure 6 shows that in both the LS and ESS, Melt Advance in spring is significantly correlated with sea ice cover in September, which is consistent with previous studies utilizing Melt Onset as a predictor of summer sea ice (Petty et al., 2017; Wang et al., 2011). However, it has no stronger prediction skill than SIC in May. In the ESS, it seems that MA performs slightly better than May SIC predicting the September

SIC. The main reason may be that May SIC in the ESS has small interannual variability, which is consistent with the lack of polynya activity in the ESS relative to the LS. Beyond this, for the prediction of summer sea ice cover, the seasonal evolution from spring to summer is still a challenge as it is not fully understood. Processes during the melting season may strongly disturb the signal from the Melt Advance (Fig. S10). More study of seasonal evolution in the Arctic is needed in the future.

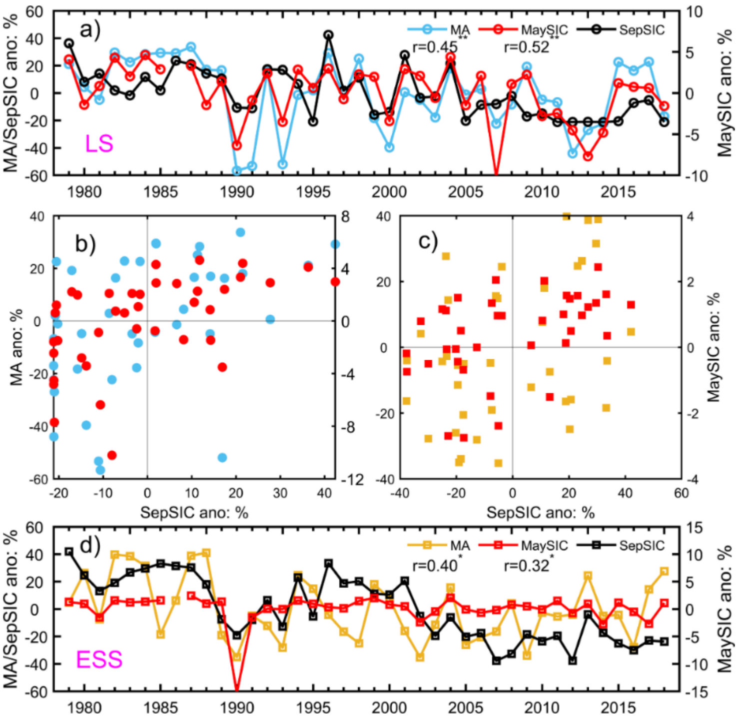

Fig. 6. Sea-ice surface Melt Advance, SIC in May and September sea ice cover in the Laptev Sea (subplot a and b) and East Siberian Sea (subplot c and d), 1979-2018. September sea ice cover is denoted by the areal percentage of sea ice cover relative to the whole sea. To facilitate viewing, Melt Advance is timed by -1. Correlation coefficients with double asterisks denote 99% confidence, while those with a single asterisk denote 90% confidence.

4. Discussion

In this study, sampling for different scenarios of sea ice Melt Advance is based on the Melt Onset dataset, which is a satellite observation product. To our knowledge, ERA5 to some extent incorporates the sea ice concentration dataset of OSI SAF, but not the Melt Onset dataset (Hersbach et al., 2020). ERA5 atmospheric reanalysis and different Melt Advance patterns can be seen as independent sources of information and their consistency should provide more confidence.

In fact, the concept of Melt Advance can be used for the whole Arctic, and can describe how sea-ice surface melting advances in spring. As mentioned above, Melt Advance can also be used as relatively independent information with reference to an atmospheric reanalysis dataset. Liang and Zhou (2023) identified three modes of Melt Onset in the LS and ESS by EOF decomposition. The positive L-mode and E-mode in their study correspond to LS-faster-scenario and ESS-faster-scenario, while the positive and negative LE-mode relate to fast-scenario and slow-scenario, respectively.

Regarding SIC anomaly in the LS and ESS, we should bear in mind that before melting the shelf areas of the LS and ESS are covered with extensive fast ice (up to 200 km wide), which is formed by April (Selyuzhenok et al., 2015). SIC in May can increase due to specific wind fields, but it probably does not consolidate against the land. Instead, the SIC anomaly is closely related to polynya development. As Fig. 3 shows, the largest SIC anomaly under the four scenarios usually occurs around the polynya region (Willmes et al., 2011).

5. Conclusions

In this study, the metric of Melt Advance (MA) is used to measure sea-ice surface melting instead of region-mean Melt Onset. MA is defined as the areal percentage of a sea in which the sea ice surface has begun to melt at the end of May, in this case the Laptev Sea (LS) and East Siberian Sea (ESS). This metric has the potential to help seasonally predict summer sea ice for the whole Arctic.

Four representative scenarios of Melt Advance in the LS and ESS are identified: the ESS-faster-scenario, LS-faster-scenario, slow-scenario, and fast-scenario. Composite analyses reveal that in these distinct scenarios of Melt Advance, atmospheric circulation, sea ice dynamics (polynya activities), air mass advection, and surface energy fluxes are related with each other. ESS-faster-scenario is associated with positive TWV anomaly over the ESS and negative TWV anomaly over the LS. LS-faster-scenario and fast-scenario seem to occur when polynya in the Laptev Sea opens. But the slow-scenario mainly reflect the cool Arctic state in the 1980s. In addition, polynya activity in this region and initial sea ice condition are also not neglectable. The main conclusions are demonstrated in the schematic of Fig. 7.

Although sea ice Melt Advance as well as sea ice cover in May are both statistically correlated with sea ice cover in September, seasonal evolution can to a large extent disturb this linkage. This study suggests a need to further investigate the changeable spring circulation in the lower troposphere and seasonal evolution in the Arctic.

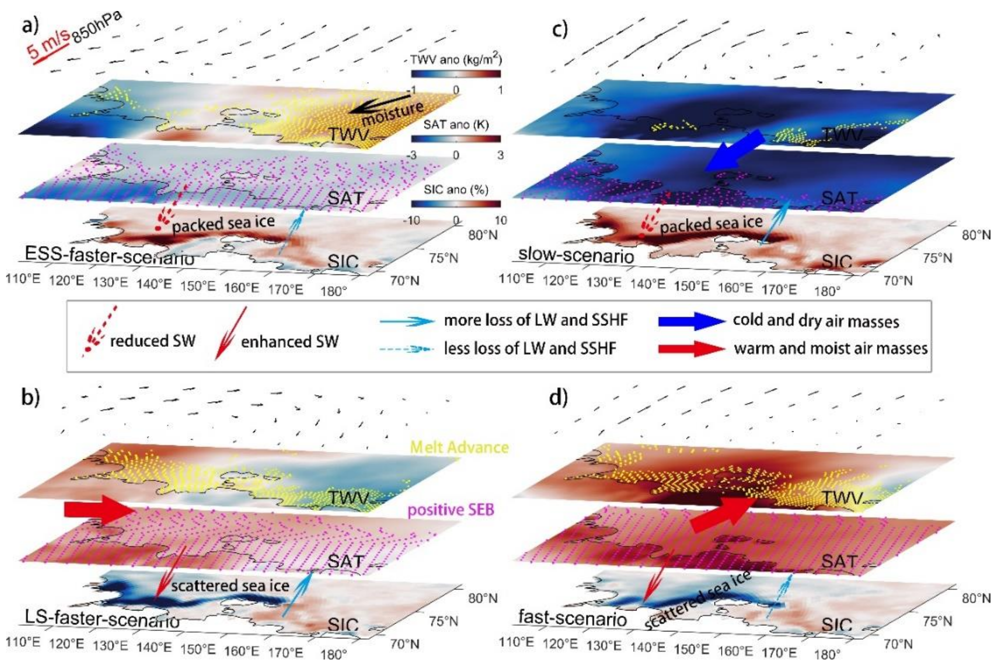

Fig. 7. Schematic processes under the four scenarios of sea ice Melt Advance in the LS and ESS. a) ESS-faster-scenario; b) LS-faster-scenario; c) slow-scenario; d) fast-scenario. For each scenario, four layers represent composite anomalies of wind fields at 850 hPa, TWV, SAT, and SIC, respectively. Thin arrows denote shortwave radiation (red), and longwave radiation and sensible heat flux (cyan), while solid and dashed types suggest the fluxes enhanced or weakened. Bold blue arrow refers to transport of cold and dry air masses, while bold red arrow refers to warm and moist advection. Yellow dots superimposed upon TWV show Melt Advance by the end of May. Magenta dots upon SAT denote positive surface energy balance (SEB).

Data Availability Statement.

The sea ice MO dataset is from NASA's Cryospheric Sciences Research Portal (https://earth.gsfc.nasa.gov/cryo/data/arctic-sea-ice-melt). SAT of IABP/POLES can be accessed at https://arcticdata.io/catalog/view/doi:10.18739/A2J598, and SAT of AIRS at https://disc.gsfc.nasa.gov/datasets/AIRS3STD_006/summary. The SIC dataset of OSI SAF was downloaded from the websites below: ftp://osisaf.met.no/reprocessed/ice/conc/v2p0/ and ftp://osisaf.met.no/reprocessed/ice/conc-cont-reproc/v2p0/. The ERA5 reanalysis dataset was retrieved at https://cds.climate.copernicus.eu/cdsapp#!/search?type=dataset&keywords=((%20%22Product%20type:%20Reanalysis%22%20). In this study, we used ERA5 monthly averaged data at single level and pressure levels.

Author Contribution

Hongjie Liang [Formal analysis; Writing original draft].

Wen Zhou [Funding acquisition; Supervision].

Competing interests

The authors declare that they have no conflict of interest.

Acknowledgments.

This work was supported by the National Natural Science Foundation of China (Grant No. 42288101, 42120104001).

REFERENCES

Bliss, A. and Anderson, M.: Snowmelt onset over Arctic sea ice from passive microwave satellite data: 1979–2012, The Cryosphere, 8, 2089-2100, 10.5194/tc-8-2089-2014, 2014.

Budyko, M. I.: The effect of solar radiation variations on the climate of the Earth, Tellus, 21, 611-619, 10.1111/j.2153-3490.1969.tb00466.x, 1969.

Cavalieri, D., Parkinson, C., Gloersen, P., and Zwally, H.: Sea ice concentrations from Nimbus-7 SMMR and DMSP SSM/I passive microwave data, National Snow and Ice Data Center, Boulder, Colorado, USA, 10.5067/8GQ8LZQVL0VL, 1996.

Cohen, J., Screen, J. A., Furtado, J. C., Barlow, M., Whittleston, D., Coumou, D., Francis, J., Dethloff, K., Entekhabi, D., Overland, J., and Jones, J.: Recent Arctic amplification and extreme mid-latitude weather, Nature Geoscience, 7, 627-637, 10.1038/ngeo2234, 2014.

Crawford, A. D., Horvath, S., Stroeve, J., Balaji, R., and Serreze, M. C.: Modulation of Sea Ice Melt Onset and Retreat in the Laptev Sea by the Timing of Snow Retreat in the West Siberian Plain, Journal of Geophysical Research: Atmospheres, 123, 8691-8707, 10.1029/2018jd028697, 2018.

Drobot, S. D. and Anderson, M. R.: An improved method for determining snowmelt onset dates over Arctic sea ice using scanning multichannel microwave radiometer and Special Sensor Microwave/Imager data, Journal of Geophysical Research: Atmospheres, 106, 24033-24049, 10.1029/2000JD000171, 2001.

Francis, J. A. and Vavrus, S. J.: Evidence for a wavier jet stream in response to rapid Arctic warming, Environmental Research Letters, 10, 10.1088/1748-9326/10/1/014005, 2015.

Hersbach, H., Bell, B., Berrisford, P., Hirahara, S., Horányi, A., Muñoz‐Sabater, J., Nicolas, J., Peubey, C., Radu, R., Schepers, D., Simmons, A., Soci, C., Abdalla, S., Abellan, X., Balsamo, G., Bechtold, P., Biavati, G., Bidlot, J., Bonavita, M., Chiara, G., Dahlgren, P., Dee, D., Diamantakis, M., Dragani, R., Flemming, J., Forbes, R., Fuentes, M., Geer, A., Haimberger, L., Healy, S., Hogan, R. J., Hólm, E., Janisková, M., Keeley, S., Laloyaux, P., Lopez, P., Lupu, C., Radnoti, G., Rosnay, P., Rozum, I., Vamborg, F., Villaume, S., and Thépaut, J. N.: The ERA5 global reanalysis, Quarterly Journal of the Royal Meteorological Society, 146, 1999-2049, 10.1002/qj.3803, 2020.

Horvath, S., Stroeve, J., Rajagopalan, B., and Jahn, A.: Arctic sea ice melt onset favored by an atmospheric pressure pattern reminiscent of the North American-Eurasian Arctic pattern, Climate Dynamics, 57, 1771-1787, 10.1007/s00382-021-05776-y, 2021.

Kashiwase, H., Ohshima, K. I., Nihashi, S., and Eicken, H.: Evidence for ice-ocean albedo feedback in the Arctic Ocean shifting to a seasonal ice zone, Sci Rep, 7, 8170, 10.1038/s41598-017-08467-z, 2017.

Krumpen, T., Hölemann, J. A., Willmes, S., Morales Maqueda, M. A., Busche, T., Dmitrenko, I. A., Gerdes, R., Haas, C., Heinemann, G., Hendricks, S., Kassens, H., Rabenstein, L., and Schröder, D.: Sea ice production and water mass modification in the eastern Laptev Sea, Journal of Geophysical Research, 116, 10.1029/2010jc006545, 2011.

Lavergne, T., Sørensen, A. M., Kern, S., Tonboe, R., Notz, D., Aaboe, S., Bell, L., Dybkjær, G., Eastwood, S., Gabarro, C., Heygster, G., Killie, M. A., Brandt Kreiner, M., Lavelle, J., Saldo, R., Sandven, S., and Pedersen, L. T.: Version 2 of the EUMETSAT OSI SAF and ESA CCI sea-ice concentration climate data records, The Cryosphere, 13, 49-78, 10.5194/tc-13-49-2019, 2019.

Lei, R., Cheng, B., Hoppmann, M., Zhang, F., Zuo, G., Hutchings, J. K., Lin, L., Lan, M., Wang, H., Regnery, J., Krumpen, T., Haapala, J., Rabe, B., Perovich, D. K., and Nicolaus, M.: Seasonality and timing of sea ice mass balance and heat fluxes in the Arctic transpolar drift during 2019–2020, Elementa: Science of the Anthropocene, 10, 10.1525/elementa.2021.000089, 2022.

Liang, H. and Su, J.: Variability in Sea Ice Melt Onset in the Arctic Northeast Passage: Seesaw of the Laptev Sea and the East Siberian Sea, Journal of Geophysical Research: Oceans, 126, e2020JC016985, 10.1029/2020JC016985, 2021.

Liang, H. and Zhou, W.: Arctic Sea Ice Melt Onset in the Laptev Sea and East Siberian Sea in Association with the Arctic Oscillation and Barents Oscillation, Journal of Climate, 36, 6363-6373, 10.1175/jcli-d-22-0791.1, 2023.

Markus, T., Stroeve, J. C., and Miller, J.: Recent changes in Arctic sea ice melt onset, freezeup, and melt season length, Journal of Geophysical Research (Oceans), 114, C12024, 10.1029/2009jc005436, 2009.

Mortin, J., Svensson, G., Graversen, R. G., Kapsch, M.-L., Stroeve, J. C., and Boisvert, L. N.: Melt onset over Arctic sea ice controlled by atmospheric moisture transport, Geophysical Research Letters, 43, 6636-6642, 10.1002/2016GL069330, 2016.

Petty, A. A., Kurtz, N. T., Kwok, R., Markus, T., and Neumann, T. A.: Winter Arctic Sea Ice Thickness From ICESat‐2 Freeboards, Journal of Geophysical Research: Oceans, 125, 10.1029/2019jc015764, 2020.

Petty, A. A., Schröder, D., Stroeve, J. C., Markus, T., Miller, J., Kurtz, N. T., Feltham, D. L., and Flocco, D.: Skillful spring forecasts of September Arctic sea ice extent using passive microwave sea ice observations, Earth's Future, 5, 254-263, 10.1002/2016ef000495, 2017.

Screen, J. A. and Simmonds, I.: The central role of diminishing sea ice in recent Arctic temperature amplification, Nature, 464, 1334-1337, 10.1038/nature09051, 2010.

Sellers, W. D.: A Global Climatic Model Based on the Energy Balance of the Earth-Atmosphere System, Journal of Applied Meteorology and Climatology, 8, 392-400, 10.1175/1520-0450(1969)008<0392:agcmbo>2.0.co;2, 1969.

Selyuzhenok, V., Krumpen, T., Mahoney, A., Janout, M., and Gerdes, R.: Seasonal and interannual variability of fast ice extent in the southeastern Laptev Sea between 1999 and 2013, Journal of Geophysical Research: Oceans, 120, 7791-7806, 10.1002/2015jc011135, 2015.

Serreze, M. C., Barrett, A. P., Stroeve, J. C., Kindig, D. N., and Holland, M. M.: The emergence of surface-based Arctic amplification, The Cryosphere, 3, 11-19, 10.5194/tc-3-11-2009, 2009.

Skeie, P.: Meridional flow variability over the Nordic Seas in the Arctic oscillation framework, Geophysical Research Letters, 27, 2569-2572, 10.1029/2000gl011529, 2000.

Stroeve, J. and Notz, D.: Changing state of Arctic sea ice across all seasons, Environmental Research Letters, 13, 103001, 10.1088/1748-9326/aade56, 2018.

Stroeve, J. C., Markus, T., Boisvert, L., Miller, J., and Barrett, A.: Changes in Arctic melt season and implications for sea ice loss, Geophysical Research Letters, 41, 1216-1225, 10.1002/2013gl058951, 2014.

Taylor, P. C., Boeke, R. C., Boisvert, L. N., Feldl, N., Henry, M., Huang, Y., Langen, P. L., Liu, W., Pithan, F., Sejas, S. A., and Tan, I.: Process Drivers, Inter-Model Spread, and the Path Forward: A Review of Amplified Arctic Warming, Frontiers in Earth Science, 9, 10.3389/feart.2021.758361, 2022.

Wang, L., Wolken, G. J., Sharp, M. J., Howell, S. E. L., Derksen, C., Brown, R. D., Markus, T., and Cole, J.: Integrated pan-Arctic melt onset detection from satellite active and passive microwave measurements, 2000-2009, Journal of Geophysical Research: Atmospheres, 116, 10.1029/2011jd016256, 2011.

Willmes, S., Adams, S., Schröder, D., and Heinemann, G.: Spatio-temporal variability of polynya dynamics and ice production in the Laptev Sea between the winters of 1979/80 and 2007/08, Polar Research, 30, 10.3402/polar.v30i0.5971, 2011.